## PAPER

# Functionalization of rare-earth nanoparticles with hybrid silica-lipid shells for T-cell labeling

Swati Kataria [ID] [a] and Angela M. Belcher [ID] *[b,c,d]

Lanthanide-doped nanophosphors are an emergent class of optical materials very attractive for biological imaging as they offer deep tissue penetration lengths, high contrast and minimal autofluorescence. An exciting and relatively unexplored application of these nanoparticles is the ability to label and track immune cell populations non-invasively. However, biological application of these nanoparticles is often limited by the challenges in surface functionalization of these nanocrystals. In this study, we engineer methods to functionalize $NaYF_4$ (Yb, Er) nanoparticles with hybrid silica-lipid shells and demonstrate successful and stable labelling of immune cells (T-lymphocytes) for the formation of near-infrared fluorescent immune cells. We use super-resolution microscopy to characterize cell labeling at nanoscale resolution and show individual nanoparticles bound or internalized to T-cells. These surface medication methods are modular and customizable to enable targeting to a variety of cell types, with the potential for broad applications in a variety of disease phenomena such as non-invasive visualization of cell-based therapies.

## Introduction

Rare-earth nanoparticles, also known as lanthanide-doped nanophosphors and upconversion/downconversion nanoparticles are an emerging class of optical nanomaterials that are very attractive for biomedical imaging applications. Emission in the NIR-II region (>1000 nm) confers deep tissue penetration lengths, and a large anti-Stokes shift allows clear separation of excitation and emission wavelengths unlike most dyes and fluorophores. RENPs are highly photostable making them ideal candidates for longitudinal imaging, and their narrow emission bands can be tuned with a variety of dopants suitable for multiplexed *in vivo* imaging.[1,2] In a direct comparison, RENPs outperformed quantum dots, carbon nanotubes, and an organic NIR dye in terms of image resolution and clarity.[3]

An exciting and relatively unexplored application of these nanoparticles is the ability to track small and rare cell populations, such as immune cells. With the emergence of cancer immunotherapy in the past decade as a promising treatment approach to cancer, immune cells like T-cells and NK-cells that

drive anti-tumor response have become an increasingly active area of research. Many immunotherapies leverage engineered T-cells like chimeric-antigen receptor (CAR) T-cells that are adoptively transferred to patients to target cancer cells.[4] However, response rates to immunotherapies remain limited,[5,6] with tumor infiltration by cytotoxic T-cells (CD8+ T-cells) being a key prognostic indicator of response status.[7,8] Therefore, tumors that cannot support infiltration of these cytotoxic or engineered T-cells may not respond to treatment, requiring other interventions. A theranostic approach that enables visualization of this key response characteristic (without resorting to invasive tumor biopsies) can provide valuable insight into response status and enable tailoring of treatment in real-time.

Nearly all reported methods for RENP synthesis yield nanoparticles capped with oleic acid dispersed in organic solvents,[9-11] which poses a challenge for subsequent biological applications. Generating a stable hydrophilic surface coating on the oleic acid capped hydrophobic nanocrystals to enable aqueous stability and biofunctionalization is a critical component of making these RENPs biocompatible. It is not a trivial issue, and many different materials, ranging from polymers, silica, lipids, and proteins have been used to engineer surface coatings with varying degrees of success, difficulty, and reproducibility.[12-14] Since the final size, dispersity, and aqueous stability of these RENP dispersions is critical for subsequent *in vivo* work, we engineered new processes for phase transfer enable facile downstream protein functionalization.

*[a]Harvard-MIT Division of Health Sciences and Technology, Massachusetts Institute of Technology, Cambridge, MA 02139, USA*
*[b]Koch Institute for Integrative Cancer Research, Massachusetts Institute of Technology, Cambridge, MA 02142, USA. E-mail: belcher@mit.edu*
*[c]Department of Biological Engineering, Massachusetts Institute of Technology, Cambridge, MA 02139, USA*
*[d]Department of Materials Science and Engineering, Massachusetts Institute of Technology, Cambridge, MA 02139, USA*

Most work in the field of RENP bioimaging has leveraged Er based nanocrystals, specifically $NaYF_4$ co-doped with Yb atoms as sensitizers and Er atoms as emitters.[3,11] We used a thermal decomposition method from Dang *et al.*[3] to synthesize β-phase $NaYF_4$ (20% Yb and 2% Er) nanocrystals for subsequent functionalization. We then present novel methods to functionalize these nanoparticles with hybrid silica-lipid shells, and demonstrate successful and stable labelling of CD8+ T-cells (using both covalent and non-covalent methods) for the formation of NIR-II fluorescent T-cells that can be used in downstream applications.

## Results and discussion

### Generation of silica shell using ligand exchange and PVP-40

The majority of published protocols that generate silica shells around RENPs use a reverse microemulsion process.[15,16] In this method, the as-synthesized RENPs are dispersed in an organic solvent (hexane or cyclohexane) with ammonia and a surfactant (IGEPAL CO-520), and TEOS (tetraethyl orthosilicate) is gradually added to the solution. The drawback to this method is that it is difficult to completely remove all the surfactant from the solution after synthesis, even after repeated and laborious washing steps in a variety of solvents. The coating process is also accompanied by the formation of bare or empty silica nanoparticles which spin down during purification and are difficult to separate from the RENPs (Fig. 1). To overcome these challenges, we devised a new strategy inspired by two different papers[17,18] to generate highly monodisperse, low impurity, silica coated RENPs.

The first step in this method is removing the oleate ligand on the nanoparticle surface *via* $NOBF_4$ treatment.[17] The authors in this work propose that $NO^+$ is a good leaving group and reacts with solvated water molecules to produce nitrous acid and fluoroboric acid, which creates an acidic environment leading to protonation of the organic ligands complexed to the RENP surface. The $BF_4-$ anions thus replace the COO– groups of oleic acid, and the subsequent positively charged RENPs are easily dispersed in polar solvents like dimethylformamide (DMF). We then coat these RENPs with polyvinylpyrrolidone (PVP-40), a polymer that adsorbs to polar surfaces extremely well due to its polarity. We then adapt the procedures outlined in ref. 18, to generate uniform silica shells on RENPs in ethanol *via* the classical Stöber pathway.

After some optimizations, the following parameters were determined to yield the best outcomes for 200–300 nm $NaYF_4$ (10% Yb, 2% Er) RENPs: 2 : 1 weight ratio for PVP/RENP coating, 0.1 mg ml$^{-1}$ NP-PVP dispersion in ethanol, with 4.2% ammonia, and a final concentration of 0.224 mM TEOS. The overall schematic of this process is shown in Fig. 1A.

This method also allows us to incorporate fluorescent dye molecules into the silica shell during the synthesis process. Incubating an amine-containing TEOS variant such as aminopropyltriethoxysilane (APTES) with an amine-reactive NHS dye generates a fluorescent TEOS variant that can be covalently incorporated into the silica matrix. We found that doping 2–3% of this fluorescent silane was sufficient to produce intensely colored RENP nanoparticles that showed no difference in size and dispersity to the uncolored variants. This fluorescent label allows us to visualize the RENPs in subsequent flow cytometry and microscopy studies.

The final nanoparticles show extremely uniform ~10 nm thick shells (thickness can be varied by adding more or less TEOS) on TEM without any impurities due to surfactants or 'empty' silica nanoparticles (Fig. 1B). In comparison, the reverse microemulsion method[15] on identical RENPs yields uneven silica shells with a lot of extraneous small silica nanoparticles stuck to the RENPs that cannot be separated easily. DLS measurements show nanoparticles with an exceptional polydispersity index (0.056) and a size distribution that agrees with TEM measurements (Fig. 1D). The RENPs also exhibit a strong negative zeta potential (−28 mV) characteristic of negatively charged silica surfaces (Fig. 3B).

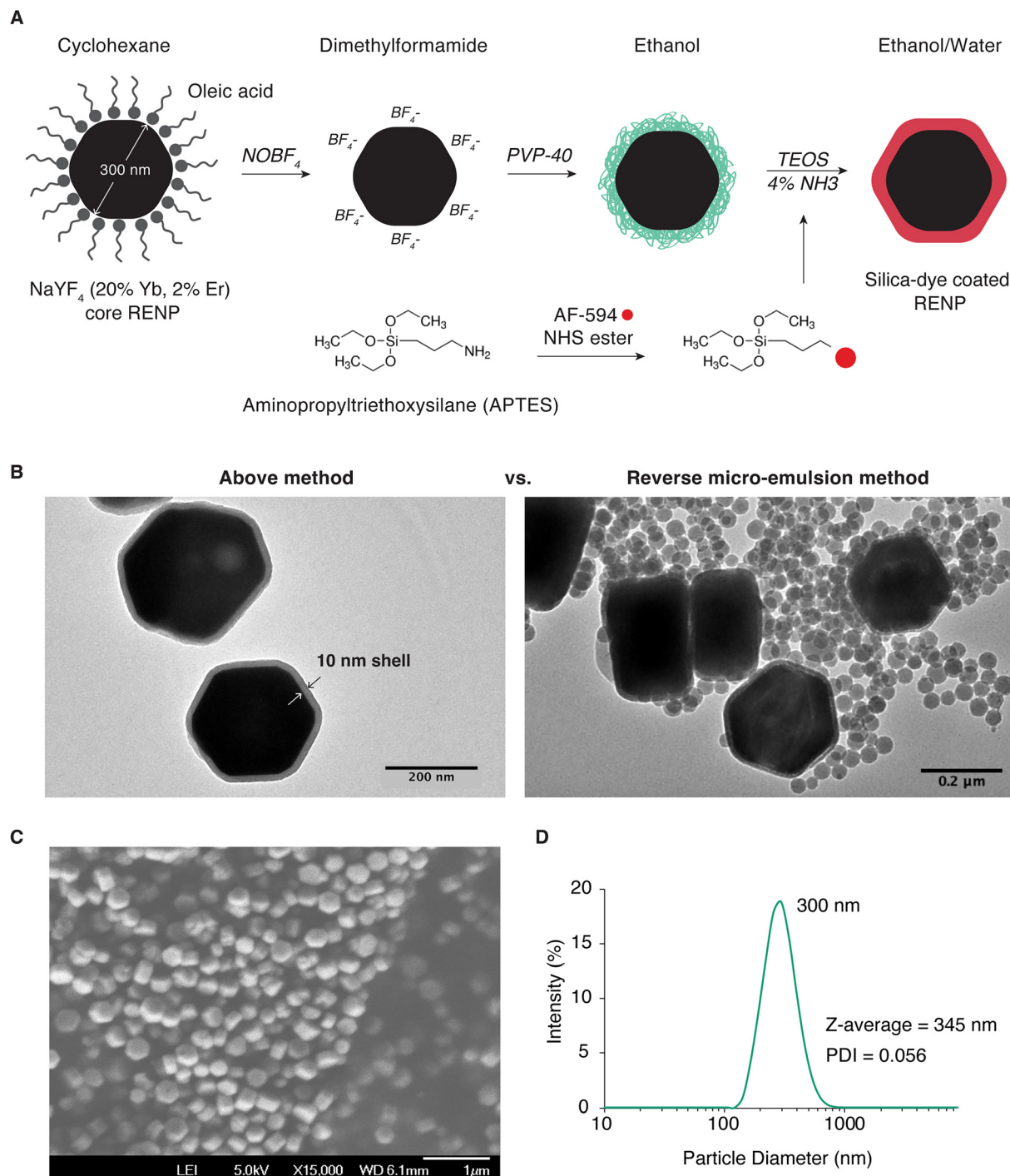### Silica-RENPs with adsorbed antibody for cell labeling

Silica surfaces are highly amenable to protein adsorption without any further modifications. We iterated through various silica functionalization reagents to introduce further functional groups that enable covalent attachment of antibodies on the RENPs, such as amines (aminopropyl-trimethoxysilane and aminopropyl-triethoxysilane), thiols (mercaptopropyl-trimethoxysilane), and azides (azidopropyl-trimethoxysilane). However, we achieved the strongest cell labeling through simple adsorption of the antibodies on the nanoparticle surface. This finding is supported by a study[19] that evaluated antibody adsorption on polystyrene nanoparticles and found that the adsorbed antibody was more efficient at binding to its target cells than the covalently attached antibody despite the formation of a protein corona *in vivo*.

Adsorption is easily achieved through simple incubation of the RENPs and targeting antibody for 1 h. The only drawback here is that spin-purification of these complexes in our work leads to aggregation, but given the high affinity of the protein to the silica surface, a large excess of antibody is not required and high labeling can be achieved even without purification.

We used the anti-CD3 antibody for targeting, which has been shown to induce internalization of CD3-antibody coated nanoparticles by their target T-cells.[20] We incubated RENP-CD3 complexes with *ex vivo* activated CD8+ T-cells for 1 h at 37 °C (1000–5000 RENPs per cell, see Methods for calculations of absolute RENPs from mass), and then washed the cells several times with PBS to remove the unconjugated nanoparticles. We analyzed the viability of the T-cells *via* flow cytometry and evaluated NP-labeling *via* the Alexa Fluor 594 fluorophore embedded in the silica shell. Half of the labelled cells were resuspended back in complete media, kept back in the incubator, and analyzed the next day to evaluate the stability of the NP association with the T-cells over 24 h.

The labelled T-cells showed high viability, identical to the control T-cells, showing that the RENP-IgG complexes have very low toxicity (Fig. 2B). The % of T-cells labelled increases
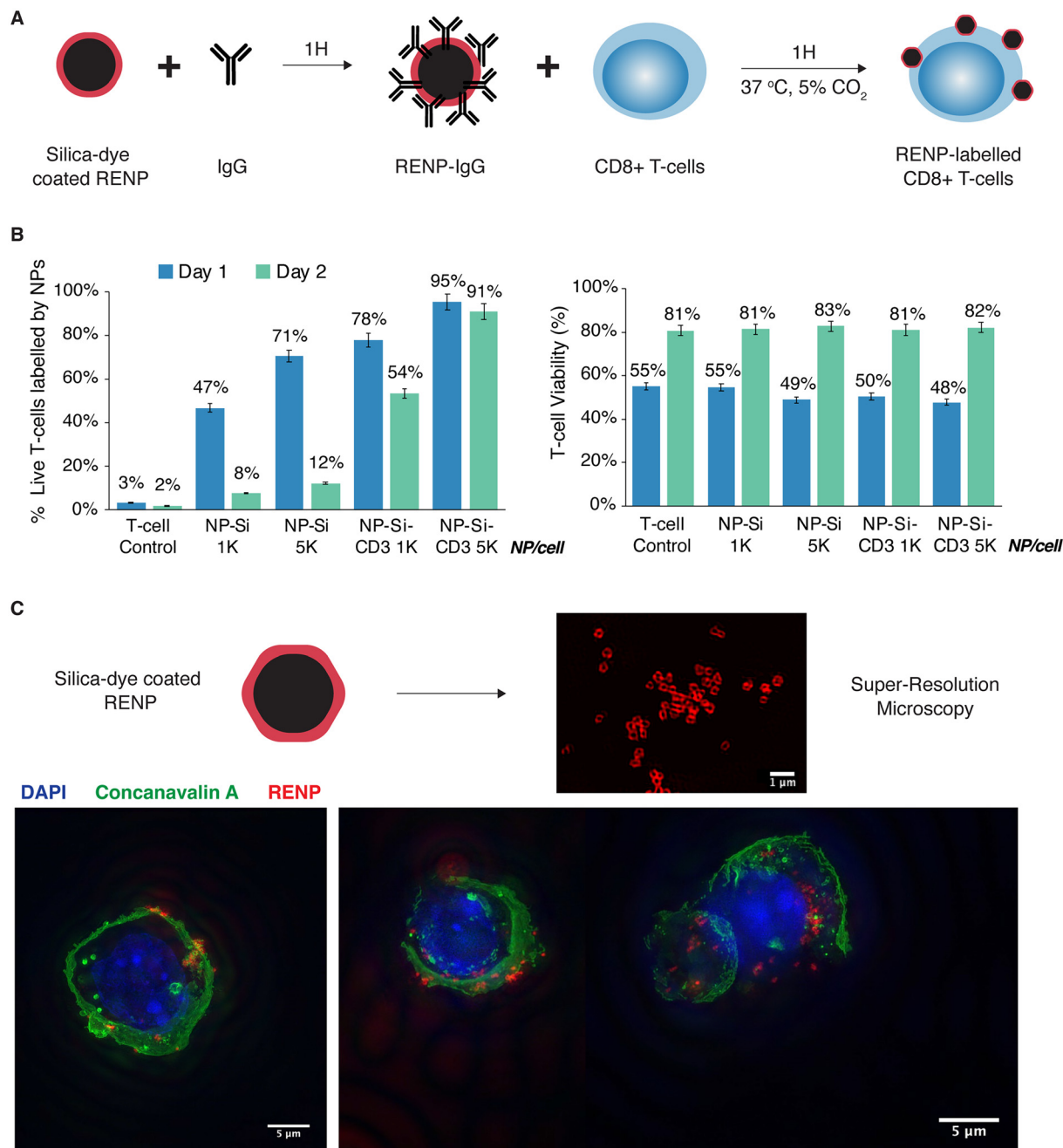
**Fig. 1** Silica functionalization of RENPs. (A) Schematic of the RENP phase transfer and functionalization process. (B) TEM image (left) shows final RENPs with a 10 nm silica shell obtained using method (A) compared to TEM image (right) with silica-coated RENPs obtained using reverse micro-emulsion process. (C) SEM image of silica-coated RENPs using method (A). (D) DLS measurements showing particle diameter and PDI as measured in water at 1 mg ml$^{-1}$. Similar results were obtained for $n > 3$ independent experiments.

with concentration as expected, with 5k NPs per cell showing the highest labeling at ~95% with no loss of viability. We also observe that while free RENPs (without any antibody attached) showed some non-specific binding to the T-cells on Day 1, stable *in vitro* labelling on Day 2 was only achieved with the CD3-coated particles, with ~91% of the T-cells retaining the NPs after 24 h (Fig. 2B).

Super-resolution microscopy enables high resolution imaging of the RENPs attached to the T-cells (stained with DAPI for the nucleus and Concanavalin A-FITC for the cell

**Fig. 2** T-cell labeling with anti-CD3-adsorbed-RENPs. (A) Schematic showing the generation of anti-CD3-adsorbed-RENPs after 1 h incubation in 0.1× PBS using a ratio of ~1000 IgG/NP. (B) Flow cytometry data showing viability (measured by DAPI exclusion) and % live T-cells labelled with RENPs after incubation with free RENPs or CD3-RENPs (1k NPs per cell or 5k NPs per cell for 1 h at 37 °C) on Day 1 and Day 2 respectively. For Day 2 measurements, T-cells were purified after 1 h RENP incubation on Day 1, resuspended in media, and incubated at 37 °C, 5% CO2. (C) Super-resolution microscopy image of RENP-labelled CD8+ T-cells (blue = DAPI nuclear stain, green = ConA-FITC cell membrane stain, red = RENPs).

membrane). The NPs appear distinctly doughnut shaped as the fluorophore is only embedded in the silica shell surrounding the RENP core (Fig. 2C). We were able to clearly visualize individual RENPs (in red) attached to the T-cells, confirming the labeling evidence we see on FACS.

Based on the TEM characterization, these nanoparticles are hexagonal prisms with approximate dimensions of 250 nm diameter ($2r$) and 125 nm height ($h$), leading to surface area $A = 6rh + 3\sqrt{3}r^2 = 1.75 \times 10^5 \text{ nm}^2$. If we assume a circular antibody molecule with 10 nm diameter and idealized surface coverage, then the number of antibody molecules needed to fully cover the surface will be ~2228. The actual number may be higher as not all IgG molecules may lie flat, but it yields an estimate of the IgG/RENP ratio.

## Silica-RENPs with cationic lipid coating for cell labeling

Cationic (positively charged) lipids and polymers are widely used as cellular transfection reagents as they bind rapidly to the negatively charged cell-membrane and induce internalization of the nanocarrier (through several mechanisms like lipid fusion and endocytosis).[21] As the silica-coated nanoparticles are negatively charged, we investigated whether a cationic lipid coating can enable binding and internalization of the RENPs by T-cells through similar mechanisms.

We first generated a cationic lipid coating on the silica-coated RENPs using a mixture of 75% DOTAP, 2% DSPE-PEG$_{2000}$, and 23% cholesterol using the thin-film hydration method (Fig. 3A). After spin purification, the resultant nanoparticles show a small increase in size but a complete flipping of the zeta potential, going from −28 mV to +30 mV in water (Fig. 3B). TEM imaging reveals that the presence of a 'membrane' like coating on the otherwise smooth silica coated RENPs (Fig. 3C). The presence of a lipid layer under electron microscopy can add noise to the image making it challenging to quantify exact thickness of the coating, but it appears broadly consistent with the previous 10 nm thick layer, although a minor degree of silica loss from hydrolysis and/or sonication during the lipid coating process cannot be ruled out. Next, we performed T-cell incubation, flow cytometry and microscopy studies as in the previous section.

We find that using cationic lipids alone leads to a modest degree of cell labeling (~20%) and even this signal is largely shed by Day 2 (~3%) (Fig. 3D), indicating that cationic lipids are not very effective or stable at inducing RENP binding and retention. PEGylation can also non-specifically inhibit protein interactions which may impede cellular uptake and contribute to lower T-cell labeling. Importantly, these lipids were not observed to be toxic to the cells as indicated by high T-cell viability over several days. Super resolution microscopy shows T-cells with very distinct individual RENPs decorating the cell surface (Fig. 3E). Thus, we can conclude that cationic lipid RENPs can only drive a small amount of temporary labeling through electrostatic interactions, unlike the more stable antibody-driven binding in the previous section.

## Silica-RENPs with cationic lipids and covalently attached antibody for cell labeling

We decided to covalently conjugate an anti-CD3 antibody to the cationic lipid coated RENPs from the previous section to see if we could drive more stable T-cell labeling. We introduced 3% DSPE-PEG$_{2000}$-N$_3$ (azide) into the lipid coating formulation, and the antibody (anti-CD3) was modified with a DBCO-group (dibenzocyclooctyne) to enable 'click' conjugation to the RENPs (Fig. 4A). The DBCO-azide click reaction is rapid, well characterized, independent of pH and does not require any intermediate activation or catalysts. The advantage here over simply adsorbing the IgG on silica-coated RENPs is that there is a covalent link between the RENPs and the antibody, and the strong positive charge of the lipid and PEGylation enables spin purification of these RENP-IgG conjugates without aggre-

gation. We then performed T-cell incubation, flow cytometry and microscopy studies as in the previous section.
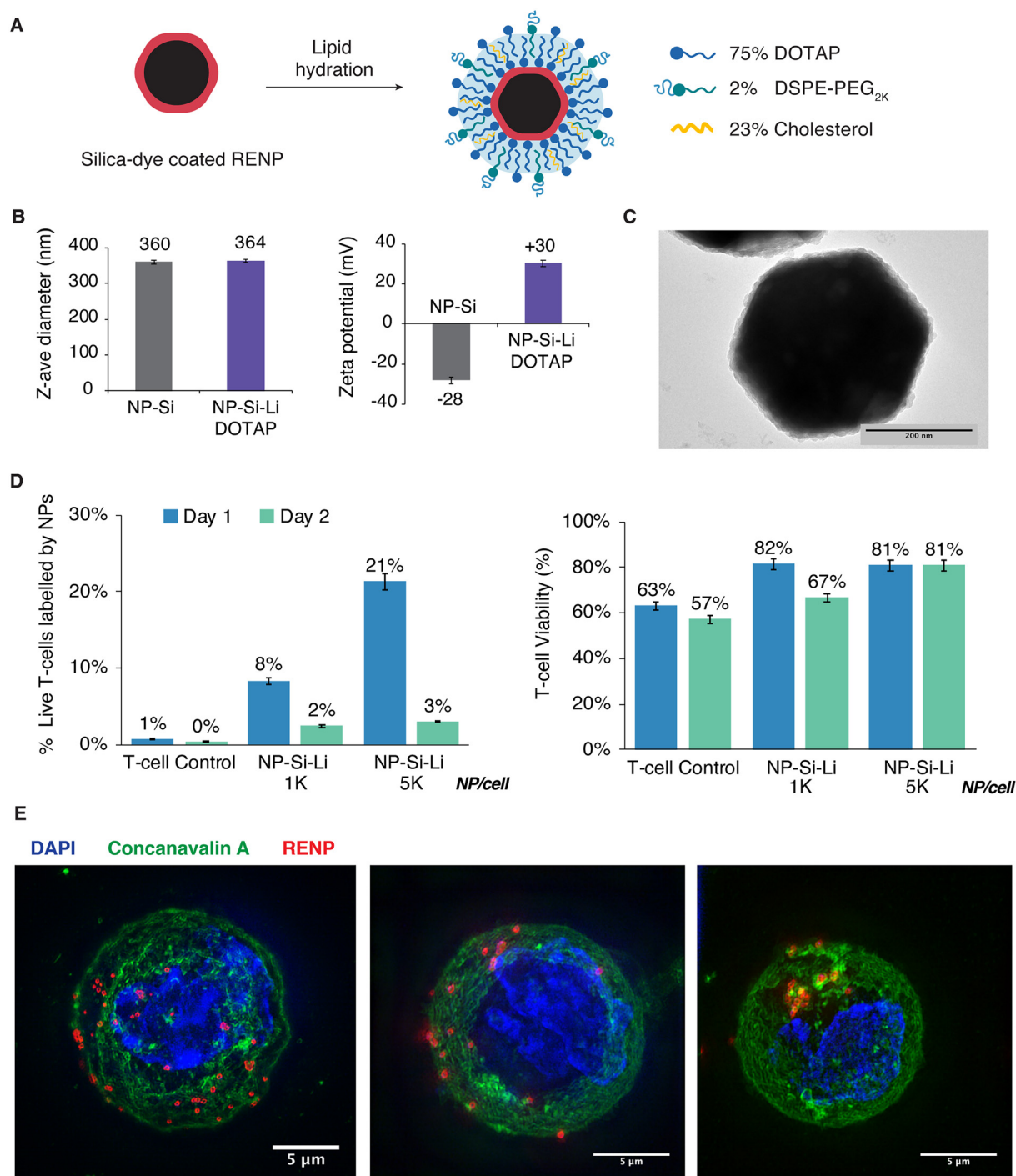
We observe that the CD3-coupled RENPs achieved 98% T-cell labeling on Day 1, and at Day 2, a remarkable 96% of the labelled T-cells retained RENP fluorescence (Fig. 4B). This labeling efficiency is comparable to what we obtained for the CD3-adsorbed RENPs (Fig. 2). There is an 8% drop in viability at high concentrations of RENPs on Day 1, which recovers to near baseline levels on Day 2, indicating once more that these RENP-lipid-antibody conjugates are not toxic to the T-cells. Super-resolution microscopy validates our flow cytometry data by showing RENPs associated with CD8+ T-cells (Fig. 4C). Visually, it appears that more RENPs in this case are internalized by the T-cells, as opposed to the more surface level binding observed in the case of cationic lipids alone (Fig. 3E). Comparing all these strategies head-to-head, we find that RENPs functionalized with a hybrid silica-lipid shell and a covalently conjugated targeting antibody enables the strongest and most stable labeling of T-cells without affecting viability.

## Discussion

Rare-earth nanoparticles have immense potential as non-invasive imaging tools at a cellular and molecular level. Their emission in the NIR-II region (>1000 nm) confers deep tissue penetration lengths (simulations suggest up to 10 cm (ref. 22)) as biological tissue in this spectral range exhibits reduced absorption and scattering of photons and extremely low autofluorescence.[22,23] They have tunable emissions enabling the generation of a wide array of imaging probes with adjustments in dopant atom concentration.[1] Importantly, they show low toxicity in a variety of animal models[24,25] and superior safety characteristics *in vivo* when compared to quantum dots, carbon nanotubes and near-infrared dyes.[3] Given that these crystals are synthesized and dispersed in organic solvents, a key challenge for biological applications is mediating phase transfer into aqueous and biological buffers without affecting nanoparticle size and dispersity.

In this work, we engineered new processes for phase transfer, surface modification, and protein functionalization of RENPs for T-cell labeling. We first developed a silica coating method that yields extremely uniform and monodisperse silica coated RENPs. This method is faster, is less laborious, enables easy fluorophore incorporation in one-step, and produces higher purity samples compared to the conventional reverse-microemulsion method. We then investigated a variety of antibody conjugation strategies using these silica RENPs, from direct antibody adsorption to hybrid silica-cationic lipid shells that enable covalent conjugation of the antibody of interest. We demonstrate *via* flow cytometry that both these methods can yield extremely high and stable (>48 h) T-cell labeling *in vitro* with little to no toxic effects on these primary T-cells. We also performed super-resolution microscopy to characterize these fluorescently labelled T-cells at nanoscale resolution showing individual RENPs attached to these T-cells. We show
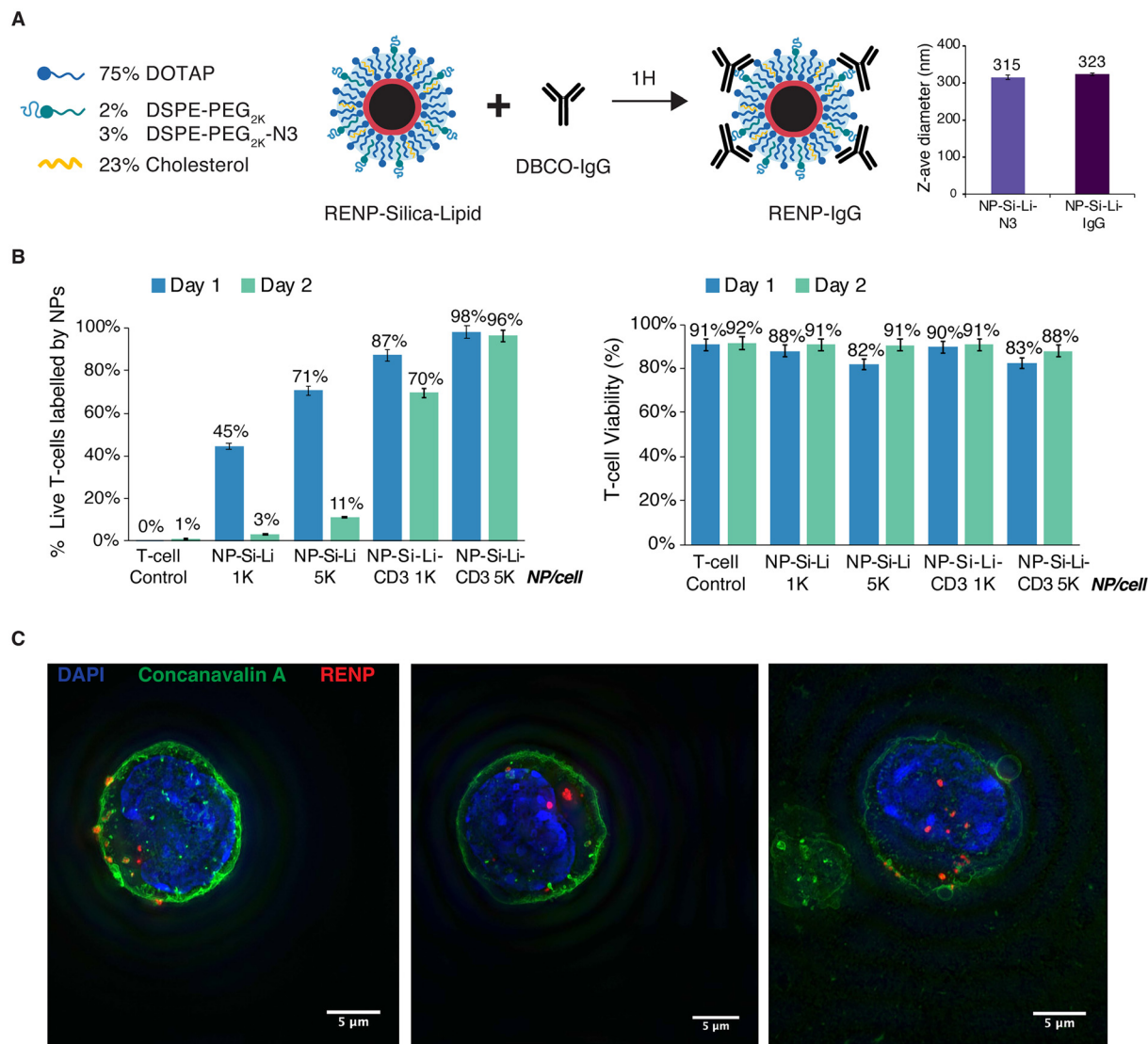
**Fig. 3** T-cell labeling with cationic lipid-coated RENPs. (A) Schematic showing the generation of cationic lipid-coated RENPs *via* lipid hydration in water. (B) DLS data comparing the Z-average diameter and zeta potential of the RENP-Silica and RENP-Silica-DOTAP complexes. (C) TEM image of a cationic lipid-coated RENP. (D) Flow cytometry data showing viability (measured by DAPI exclusion) and % live T-cells labelled with RENPs after incubation with cationic RENPs (1k NPs per cell or 5k NPs per cell for 1 h at 37 °C) on Day 1 and Day 2 respectively. For Day 2 measurements, T-cells were purified after 1 h RENP incubation on Day 1, resuspended in media, and incubated at 37 °C, 5% CO₂. (E) Super-resolution microscopy image of RENP-labelled CD8+ T-cells (blue = DAPI nuclear stain, green = ConA-FITC cell membrane stain, red = RENPs).

that while simple adsorption of antibody onto RENP-silica can enable rapid conjugation of RENPs to cells of interest, a hybrid silica-lipid shell with a covalently attached antibody enables stronger, more stable labeling of T-cells (with the ability to purify excess antibody without aggregation). Given the sensitivity of primary T-cells to culture conditions and perturbations, viability assessments using flow cytometry especially over 48 h serve as good indicators of nanoparticle mediated

**Fig. 4** T-cell labeling with cationic lipid and anti-CD3 coated RENPs. (A) Schematic showing the coupling of cationic lipid coated RENP with DBCO-modified antibody *via* DBCO-azide click chemistry with DLS size measurements (*Z*-average diameter) of the nanoparticles pre- and post-IgG conjugation. (B) Flow cytometry data showing viability (measured by DAPI exclusion) and % live T-cells labelled with RENPs after incubation with free RENPs or CD3-RENPs (1k NPs per cell or 5k NPs per cell for 1 h at 37 °C) on Day 1 and Day 2 respectively. For Day 2 measurements, T-cells were purified after 1 h RENP incubation on Day 1, resuspended in media, and incubated at 37 °C, 5% CO₂. (C) Super-resolution microscopy image of RENP-labelled CD8+ T-cells (blue = DAPI nuclear stain, green = ConA-FITC cell membrane stain, red = RENPs).

non-specific toxicity. RENPs are exceptionally inert in biological contexts,[25] but a functional immune study looking a target cell killing and cytokine production by these RENP-labelled T-cells can be an area of future exploration.

These surface functionalization and bioconjugation strategies enable rapid and facile conjugation of NIR-II fluorescent RENPs to T-cells and can be potentially used to image cell-based immunotherapies (like CAR T-cell and NK-cell therapies). Most of these immunotherapies have poor response rates in solid tumors[6] and the technology to visualize cell trafficking using non-invasive tools can serve as a useful of real-time response.

# Materials and methods

**Materials**

Yttrium trifluoroacetate $Y(CF_3COO)_3 \cdot 3H_2O$, ytterbium trifluoroacetate $Yb(CF_3COO)_3 \cdot 3H_2O$, and erbium trifluoroacetate $Er(CF_3COO)_3 \cdot 3H_2O$ were purchased from GFS Chemicals. Sodium trifluoroacetate $Na(CF_3COO)$ and all the solvents used in synthesis were purchased from Sigma Aldrich. Nitrosyl tetrafluoroborate $(NOBF_4)$, polyvinylpyrrolidone (PVP 40k MW), tetraethylorthosilicate (TEOS), aminopropyltriethoxysilane (APTES), were purchased from Sigma Aldrich. Alexa Fluor 594 NHS ester was purchased from Thermo Fisher Scientific.

## Synthesis of RENPs

We used a thermal decomposition method from previous work[3,11] to synthesize $NaY_{0.78}F4$ doped with $Yb_{0.20}$ and $Er_{0.02}$. Briefly, 2 mmol $Na(CF_3COO)$ and 2 mmol $RE(CF_3COO)_3$ (RE = 78% Y, 20% Yb, 2% Er) were added to 5 ml ODE (octadecene) and 5 ml OA (oleic acid). This solution was heated under vacuum under constant magnetic stirring and kept at 100 °C for 45 min to form a clear yellow precursor solution. This solution was then cooled to RT for subsequent injection. In another 3-necked flask, 15 mL of ODE and 15 mL of OA were first bubbled with argon for 15 minutes and then heated to 330 °C under vigorous stirring. The yellow precursor was then injected into the boiling solvent, which generates a lot of white smoke indicating thermal decomposition of the trifluoroacetate salts. After the temperature climbs back up to 330 °C, the solution was allowed to react at 330 °C for 30 min. The solution was then cooled down and centrifuged after the addition of ethanol. The pellet was resuspended in a 4 : 1 mixture of ethanol and hexane, sonicated to dissolve large chunks, and centrifuged again. The RENPs were finally re-dispersed and stored in hexane at ~20 mg $ml^{-1}$.

## Ligand exchange with PVP

We adapted a ligand-exchange strategy[26] to mediate the transfer of the hydrophobic RENPs into polar solvents and perform polymer coating. Briefly, excess $NOBF_4$ (Sigma) was dissolved in DMF and immediately after the RENPs in hexane/cyclohexane were added to this solution. After gentle shaking for 5–10 minutes (precipitation can be observed), this solution was centrifuged (3000 rpm × 10 minutes) and the precipitate was re-dispersed in DMF to form a clear solution. For coating with PVP-40 (Sigma), the RENPs were added dropwise to a PVP-40 solution in DMF (2 mg $ml^{-1}$) at a RENP : polymer ratio of 1 : 2 by weight and vortexed for 30 minutes. Acetone was then added to precipitate the RENPs and the solution was centrifuged (3000 rpm × 10 minutes). The RENPs were finally re-dispersed in ethanol with sonication at 1 mg $ml^{-1}$ for subsequent silica coating.

## Silica coating of RENPs (via ligand exchange and PVP coating)

To make the fluorescent dye-silane conjugates, equimolar amounts of Alexa Fluor 594 NHS ester (Thermo Fisher) were mixed with APTES (Sigma) in ethanol and incubated at least overnight. The RENP-PVP solution was diluted to ~0.1 mg $ml^{-1}$ in ethanol and sonicated 10 minutes to ensure dispersity. Under vigorous stirring, ammonium hydroxide (28–30%) was added to a final concentration of 4.2%. TEOS (Sigma) was then added dropwise to a final concentration of 0.27 mM and the dye-silane conjugate was doped in at ~1.5% of the TEOS concentration (small variations in these ratios do not affect the final results). The solution was stirred overnight at RT. The RENP-silica particles were then washed in ethanol twice by centrifugation (3000 rpm × 10 minutes) and stored in ethanol at 5 mg $ml^{-1}$.

## Silica-RENPs with cationic lipid coating

75% DOTAP/2% DSPE-PEG$_{2k}$/23% cholesterol (all lipids were purchased from Avanti Polar Lipids) mixture was dried in a round bottom flask at 1.2× RENP weight. The required weight of silica-RENPs (1 mg $ml^{-1}$ in ethanol) was added to this flask, sonicated and dried to remove the ethanol. Water was added to make 0.1 mg $ml^{-1}$ RENP solution and sonicated until the solution is well dispersed (up to 1 h). The solution was then spun at 1600 rpm for 7 minutes and resuspended in water for characterization.

## Silica-RENPs with cationic lipids and covalently conjugated antibody

NHS-PEG4-DBCO (Click Chemistry Tools) was used to functionalize the anti-CD3ε antibody according to manufacturer's instructions. The RENP-Silica-Lipid-Azide complexes were incubated with the modified antibody at 1000 IgG/RENP in 10 mM HEPES buffer for 1 h and subsequently spin purified.

## Nanoparticle characterization methods

Hydrodynamic radius, PDI and zeta potentials were measured using Malvern ZS90 particle analyzer. TEM imaging was done on FEI Tecnai Multipurpose Digital TEM (120 kV) using Cu-400 copper grids (Electron Microscopy Sciences).

## Cells

T-cells were cultured in T-cell Culture Media: RPMI (Life Technologies) with 10% heat-inactivated FBS (Life Technologies), 1 mM sodium pyruvate (Life Technologies), 1× minimal essential medium (MEM) non-essential amino acids (Life Technologies), 1× Glutamax (Life Technologies), 30 U $ml^{-1}$ IL-2 (Peprotech), 0.05 mM β-mercaptoethanol (Millipore Sigma), 100 units per ml penicillin and 100 μg $ml^{-1}$ streptomycin (Life Technologies).

CD8+ T-cells were extracted from spleens of pmel (B6.Cg-Thy1a/Cy Tg(TcraTcrb)8Rest/J) mice (Jackson Labs). Briefly, spleens were mashed through a 70 μm cell strainer using a cell pestle with PBS washing to dissociate the splenocytes. The cells were pelleted (500 g × 5 min) and resuspended in 2–3 ml ACK lysis buffer (Life Technologies) for 5 minutes. PBS was added and the cells were pelleted again for subsequent CD8+ T-cell isolation using EasySep™ Mouse CD8+ T Cell Isolation Kit (StemCell Technologies) following manufacturer's instructions. After isolation, the CD8+ T-cells were resuspended in T-cell Culture Media described above and co-activated with plate-bound anti-CD3 (BioXCell) and soluble 2 μg $ml^{-1}$ anti-CD28 (BioXCell). To generate plate-bound antibody, a 6-well plate was incubated overnight at 4 °C with 2 ml per well of 10 μg $ml^{-1}$ anti-mouse CD3 and washed with PBS to remove unbound antibody.

All cell cultures were maintained at 37 °C and 5% $CO_2$ and tested regularly for mycoplasma contamination. All animal work was conducted under the approval of the Massachusetts Institute of Technology (MIT) Division of Comparative

Medicine in accordance with federal, state and local guidelines.

## Microscopy

MicroTek 8-well cover-slip bottom chambers were coated with 200 μL of 0.001% poly-L-lysine 75k–150k MW (Sigma). After 10 minutes, they were washed 3× with water and dried. 200 μL of T-cells (with or without RENPs) at $10^6$ cells per ml concentration in media were added to the chambers and incubated 37 °C and 5% $CO_2$ for 20–30 minutes. The media was gently aspirated out and the chambers were washed gently 1× with PBS. 4% paraformaldehyde was added to the chambers and incubated for 10 minutes. After aspiration, ~300 nM DAPI in PBS (Sigma) was added for 5 minutes. After aspiration again, 50 μg ml$^{-1}$ of Concanavalin A-FITC (Sigma) in PBS was added for 5 minutes. Finally, the cells were washed once with PBS and Vectashield H-1000 (Vector Labs) was added to cover the surface. The cells were stored at 4 °C until microscopy. Super-resolution imaging was done on the Applied Precision DeltaVision-OMX Super-Resolution Microscope. 100× objective was used for imaging with the excitation and emission filters listed below. Microscopy images were analyzed and processed in Fiji software.

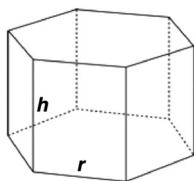| Excitation–emission | Probes & fluorochromes |
| --- | --- |
| 405/435 | DAPI |
| 488/528 | Concanavalin A – FITC |
| 594/630 | RENP – AlexaFluor594 |

## Flow cytometry

Cell staining buffer was purchased from BioLegend. For flow cytometry, cells were washed twice with PBS. $2 \times 10^5$ cells were taken from each sample and stained with DAPI (Thermo Fisher) for 10 minutes in PBS, pelleted (300 g × 5 min) and resuspended in ice-cold staining buffer for flow cytometry based viability evaluation immediately afterwards. Flow cytometry was done on BD FACS Celesta and BD FACS LSR-II. Data was analyzed using FlowJo.

## Calculation of RENP 'molecular weight'

For NaYF$_4$ hexagonal prism single nanocrystal with approximate dimensions of 250 nm diameter ($2r$) and 125 nm height ($h$):

$$\text{Volume of a nanoparticle} = \frac{3\sqrt{3}}{2}r^2h = 5.07 \times 10^6 \text{ nm}^3.$$

For hexagonal NaYF$_4$ crystals with lattice parameters $a = 0.596$ nm and $c = 0.353$ nm:[27,28]

$$\text{Volume of a hexagonal (hcp) unit cell}$$
$$= \frac{\sqrt{3}}{2}a^2c = 0.1086 \text{ nm}^3.$$

$$\text{Number of hcp unit cells per nanoparticle crystal}$$
$$= \frac{5.07 \times 10^6 \text{nm}^3}{0.1086 \text{ nm}^3} = 4.67 \times 10^7.$$

In an hcp lattice, the number of NaYF$_4$ molecules per unit cell = 1.

Therefore, the number of NaYF$_4$ molecules per nanoparticle crystal = $4.67 \times 10^7$.

With NaYF$_4$ molecular weight (20% Yb, 2% Er) = 206.28 mg mmol$^{-1}$.

Effective 'molecular weight' of RENPs = $206.28 \times 4.67 \times 10^7$ mg mmol$^{-1}$ = $9.64 \times 10^9$ mg mmol$^{-1}$.

This enables calculation of absolute number of RENPs when mass (mg) of RENP is known.

## Author contributions

S. K. performed the experimental design, synthesis and characterization of RENP complexes, T-cell labeling assays, flow cytometry, and data analysis. S. K. wrote the manuscript with supervision from A. M. B. All authors have given approval to the final version of the manuscript.

## Conflicts of interest

There are no conflicts to declare.

## Data availability

The authors confirm that the data supporting the findings of this study are available within the article. Raw data were generated at the Koch Institute Swanson Biotechnology Center in the Flow Cytometry and Microscopy Cores. Raw files supporting the findings of this study are available from the corresponding author on request.

## Acknowledgements

# References

1 F. Wang and X. Liu, Upconversion Multicolor Fine-Tuning: Visible to near-Infrared Emission from Lanthanide-Doped NaYF4 Nanoparticles, *J. Am. Chem. Soc.*, 2008, **130**(17), 5642–5643, DOI: **10.1021/ja800868a**.

2 Y. Fan, P. Wang, Y. Lu, R. Wang, L. Zhou, X. Zheng, X. Li, J. A. Piper and F. Zhang, Lifetime-Engineered NIR-II Nanoparticles Unlock Multiplexed in Vivo Imaging, *Nat. Nanotechnol.*, 2018, **13**(10), 941–946, DOI: **10.1038/s41565-018-0221-0**.

3 X. Dang, L. Gu, J. Qi, S. Correa, G. Zhang and A. M. Belcher, Layer-by-Layer Assembled Fluorescent Probes in the Second near-Infrared Window for Systemic Delivery and Detection of Ovarian Cancer, *Proc. Natl. Acad. Sci. U. S. A.*, 2016, **113**(19), 1–6, DOI: **10.1073/pnas.1521175113**.

4 C. H. June, R. S. O'Connor, O. U. Kawalekar, S. Ghassemi and M. C. Milone, CAR T Cell Immunotherapy for Human Cancer, *Science*, 2018, **359**(6382), 1361–1365, DOI: **10.1126/science.aar6711**.

5 C. Robert, J. Schachter, G. V. Long, A. Arance, J. J. Grob, L. Mortier, A. Daud, M. S. Carlino, C. McNeil, M. Lotem, J. Larkin, P. Lorigan, B. Neyns, C. U. Blank, O. Hamid, C. Mateus, R. Shapira-Frommer, M. Kosh, H. Zhou, N. Ibrahim, S. Ebbinghaus and A. Ribas, Pembrolizumab versus Ipilimumab in Advanced Melanoma, *N. Engl. J. Med.*, 2015, **372**(26), 2521–2532, DOI: **10.1056/NEJMoa1503093**.

6 B. Hou, Y. Tang, W. Li, Q. Zeng and D. Chang, Efficiency of CAR-T Therapy for Treatment of Solid Tumor in Clinical Trials: A Meta-Analysis, *Dis. Markers*, 2019, 3425291, DOI: **10.1155/2019/3425291**.

7 F. Pages, J. Galon, M. C. Dieu-Nosjean, E. Tartour, C. Sautes-Fridman and W. H. Fridman, Immune Infiltration in Human Tumors: A Prognostic Factor That Should Not Be Ignored, *Oncogene*, 2010, **29**(8), 1093–1102, DOI: **10.1038/onc.2009.416**.

8 R. S. Herbst, J. C. Soria, M. Kowanetz, G. D. Fine, O. Hamid, M. S. Gordon, J. A. Sosman, D. F. McDermott, J. D. Powderly, S. N. Gettinger, H. E. K. Kohrt, L. Horn, D. P. Lawrence, S. Rost, M. Leabman, Y. Xiao, A. Mokatrin, H. Koeppen, P. S. Hegde, I. Mellman, D. S. Chen and F. S. Hodi, Predictive Correlates of Response to the Anti-PD-L1 Antibody MPDL3280A in Cancer Patients, *Nature*, 2014, **515**(7528), 563–567, DOI: **10.1038/nature14011**.

9 X. Li, F. Zhang and D. Zhao, Highly Efficient Lanthanide Upconverting Nanomaterials: Progresses and Challenges, *Nano Today*, 2013, **8**(6), 643–676, DOI: **10.1016/j.nantod.2013.11.003**.

10 Z. Li and Y. Zhang, An Efficient and User-Friendly Method for the Synthesis of Hexagonal-Phase NaYF(4):Yb, Er/Tm Nanocrystals with Controllable Shape and Upconversion Fluorescence, *Nanotechnology*, 2008, **19**(34), 345606–345610, DOI: **10.1088/0957-4484/19/34/345606**.

11 X. Ye, J. E. Collins, Y. Kang, J. Chen, D. T. N. Chen, A. G. Yodh and C. B. Murray, Morphologically Controlled Synthesis of Colloidal Upconversion Nanophosphors and Their Shape-Directed Self-Assembly, *Proc. Natl. Acad. Sci. U. S. A.*, 2010, **107**(52), 22430–22435, DOI: **10.1073/pnas.1008958107**.

12 G. Chen, H. Qiu, P. N. Prasad and X. Chen, Upconversion Nanoparticles: Design, Nanochemistry, and Applications in Theranostics, *Chem. Rev.*, 2014, **114**(10), 5161–5214, DOI: **10.1021/cr400425h**.

13 A. Sedlmeier and H. H. Gorris, Surface Modification and Characterization of Photon-Upconverting Nanoparticles for Bioanalytical Applications, *Chem. Soc. Rev.*, 2015, **44**(6), 1526–1560, DOI: **10.1039/c4cs00186a**.

14 V. Muhr, S. Wilhelm, T. Hirsch and O. S. Wolfbeis, Upconversion Nanoparticles: From Hydrophobic to Hydrophilic Surfaces, *Acc. Chem. Res.*, 2014, **47**(12), 3481–3493, DOI: **10.1021/ar500253g**.

15 Y. Qin, Z. Dong, D. Zhou, Y. Yang, X. Xu and J. Qiu, Modification on Populating Paths of β-NaYF_4:Nd/Yb/Ho@SiO_2@Ag Core/Double-Shell Nanocomposites with Plasmon Enhanced Upconversion Emission, *Opt. Mater. Express*, 2016, **6**(6), 1942, DOI: **10.1364/ome.6.001942**.

16 M. K. Gnanasammandhan, N. M. Idris, A. Bansal, K. Huang and Y. Zhang, Near-IR Photoactivation Using Mesoporous Silica–Coated NaYF4:Yb,Er/Tm Upconversion Nanoparticles, *Nat. Protoc.*, 2016, **11**(4), 688–713, DOI: **10.1038/nprot.2016.035**.

17 A. Dong, X. Ye, J. Chen, Y. Kang, T. Gordon, J. M. Kikkawa and C. B. Murray, A Generalized Ligand-Exchange Strategy Enabling Sequential Surface Functionalization of Colloidal Nanocrystals, *J. Am. Chem. Soc.*, 2011, **133**(4), 998–1006, DOI: **10.1021/jal08948z**.

18 C. Graf, D. L. J. Vossen, A. Imhof and A. Van Blaaderen, *A General Method To Coat Colloidal Particles with Silica*, 2003. DOI: **10.1021/la0347859**.

19 M. Tonigold, J. Simon, D. Estupiñán, M. Kokkinopoulou, J. Reinholz, U. Kintzel, A. Kaltbeitzel, P. Renz, M. P. Domogalla, K. Steinbrink, I. Lieberwirth, D. Crespy, K. Landfester and V. Mailänder, Pre-Adsorption of Antibodies Enables Targeting of Nanocarriers despite a Biomolecular Corona, *Nat. Nanotechnol.*, 2018, **13**(9), 862–869, DOI: **10.1038/s41565-018-0171-6**.

20 N. Martínez-Martín, E. Fernández-Arenas, S. Cemerski, P. Delgado, M. Turner, J. Heuser, D. J. Irvine, B. Huang, X. R. Bustelo, A. Shaw and B. Alarcón, T Cell Receptor Internalization from the Immunological Synapse Is Mediated by TC21 and RhoG GTPase-Dependent Phagocytosis, *Immunity*, 2011, **35**(2), 208–222, DOI: **10.1016/j.immuni.2011.06.003**.

21 I. Wrobel and D. Collins, Fusion of Cationic Liposomes with Mammalian Cells Occurs after Endocytosis, *Biochim. Biophys. Acta, Biomembr.*, 1995, **1235**(2), 296–304, DOI: **10.1016/0005-2736(95)80017-A**.

22 A. N. Bashkatov, E. A. Genina, V. I. Kochubey and V. V. Tuchin, Optical Properties of Human Skin, Subcutaneous and Mucous Tissues in the Wavelength Range from 400 to 2000 Nm, *J. Phys. D: Appl. Phys.*, 2005, **38**(15), 2543–2555, DOI: **10.1088/0022-3727/38/15/004**.

23  S. Diao, G. Hong, A. L. Antaris, J. L. Blackburn, K. Cheng, Z. Cheng and H. Dai, Biological Imaging without Autofluorescence in the Second Near-Infrared Region, *Nano Res.*, 2015, **8**(9), 3027–3034, DOI: **10.1007/s12274-015-0808-9**.

24  L. Cheng, K. Yang, M. Shao, X. Lu and Z. Liu, In Vivo Pharmacokinetics, Long-Term Biodistribution and Toxicology Study of Functionalized Upconversion Nanoparticles in Mice, *Nanomedicine*, 2011, **6**(8), 1327–1340, DOI: **10.2217/nnm.11.56**.

25  Y. Sun, W. Feng, P. Yang, C. Huang and F. Li, The Biosafety of Lanthanide Upconversion Nanomaterials, *Chem. Soc. Rev.*, 2015, **44**(6), 1509–1525, DOI: **10.1039/c4cs00175c**.

26  A. Dong, X. Ye, J. Chen, Y. Kang, T. Gordon, J. M. Kikkawa and C. B. Murray, A Generalized Ligand-Exchange Strategy Enabling Sequential Surface Functionalization of Colloidal Nanocrystals, *J. Am. Chem. Soc.*, 2011, **133**(4), 998–1006, DOI: **10.1021/ja108948z**.

27  L. E. Mackenzie, J. A. Goode, A. Vakurov, P. P. Nampi, S. Saha, G. Jose and P. A. Millner, The Theoretical Molecular Weight of NaYF 4 :RE Upconversion Nanoparticles, *Sci. Rep.*, 2018, **8**(1), 1106, DOI: **10.1038/s41598-018-19415-w**.

28  C. Chen, N. Kang, T. Xu, D. Wang, L. Ren and X. Guo, Core–Shell Hybrid Upconversion Nanoparticles Carrying Stable Nitroxide Radicals as Potential Multifunctional Nanoprobes for Upconversion Luminescence and Magnetic Resonance Dual-Modality Imaging, *Nanoscale*, 2015, **7**(12), 5249–5261, DOI: **10.1039/C4NR07591A**.